POTENTIAL DROP CRACK GROWTH MONITORING IN HIGH TEMPERATURE BIAXIAL FATIGUE TESTS

B. P. Fitzgerald and E. Krempl
Mechanics of Materials Laboratory
Rensselaer Polytechnic Institute
Troy, New York 12180-3590

Abstract. The present work describes a procedure for monitoring crack growth in high temperature, biaxial, low cycle fatigue tests. The reversing DC potential drop equipment monitors smooth, tubular type 304 stainless steel specimens during fatigue testing. Electrical interference from an induction heater is filtered out by an analog filter and by using a long integration time. A Fourier smoothing algorithm and two spline interpolations process the large data set. The experimentally determined electrical potential drop is compared with the theoretical electrostatic potential that is found by solving Laplace's equation for an elliptical crack in a semi-infinite conducting medium. Since agreement between theory and experiment is good, the method can be used to measure crack growth to failure from the threshold of detectability.

TEST PROCEDURE

THE laboratory equipment consists of a computer-controlled MTS servohydraulic testing machine and a computerized DC potential drop system. The potential drop monitoring system was designed by the first author and consists of a constant current power supply, a passive RC filter bank, a multichannel digital voltmeter, solid state relays, and a 386 personal computer with a thermocouple board and a general purpose interface bus.

Testing is performed in strain control, using an MTS high temperature biaxial extensometer. Smooth type 304 stainless steel tubular specimens with an inside diameter of 15.1 mm and an outside diameter of 18.6 mm are tested. The wall thickness was reduced by 10% in the gauge section to promote crack initiation in that region. For the initial tests, a sinusoidal command signal with strain amplitude of $\epsilon_a = .005$ was used. In follow-on tests, shear strain control was slaved in-phase to the axial channel to achieve proportional loading, in which the axial and shear strain amplitudes were chosen so as to satisfy the relation

$$\epsilon^2_{a(eff)} = \epsilon^2_a + \frac{1}{3}\gamma^2_a, \quad \epsilon_{a(eff)} = .005.$$

Temperature is maintained at 538°C with a 10 kHz induction heater and controller. The use of thirteen type K thermocouples provides excellent coverage of the gauge section. Five thermocouples are located in the gauge section mid plane, four 12.7 mm above the mid plane, and four are located below. One thermocouple is used for heater control, two for auxiliary indication, nine for post-test compensation of the voltage data, and one for an installed ready spare. The desired temperature and temperature distribution is achieved by positioning two heating coils with a threaded reach rod system designed by the first author. To prepare for an experiment, a specimen is gripped and heated in manual control to 538°C, after which the heater is switched to automatic. The heater coils are adjusted both up, both down, together, or farther apart, as needed, using the reach rods, until a temperature distribution uniform within ±2.5°C of the desired temperature is achieved. Over the course of the test, oxidation decreases the material thermal conductivity, resulting in an axial shift in the temperature distribution; however, no channel changes by more than 3.5°C from its starting value.

A constant 12A direct current is passed through the specimen. The potential drop is measured across the gauge section with nine voltage probe pairs connected to a multichannel digital voltmeter, and stored on the 386 personal computer. The voltage probes consist of two 0.127 mm diameter chromel wires spot welded to the specimen surface (Figure 1). To allow for placement of the extensometer and the thermocouples, the potential drop leads are arranged in

three equally spaced groups of three. Electrical noise originating from the induction heater is largely eliminated by an RC filter bank and by using a long voltmeter integration time. Care is taken to electrically insulate the upper specimen grip from the load frame to eliminate DC current leakage. In order to compensate for the thermocouple potential arising from minor changes in gauge section temperature gradients, the current is reversed after every reading, using the solid state relays, and the voltages are remeasured. This is called the reversing DC electrical potential drop method [1]. After reversing the current, it is necessary to wait 0.5 s for the RC filter transient to decay before remeasuring the potential drop. Allowing time for passive filter decay and voltmeter integration, four seconds are required to obtain the positive and negative voltage readings. Mechanical test data (axial load, torque, axial and shear strain, and command signal), the cycle count, elapsed time, and thermocouple channel readings are recorded in synchronization with the potential drops. Approximately five samples are taken per cycle. To minimize the impact of aliasing on the data, the mechanical cycling frequency (0.04833 Hz) was selected so that the sampling frequency (0.25 Hz) is not an exact multiple.

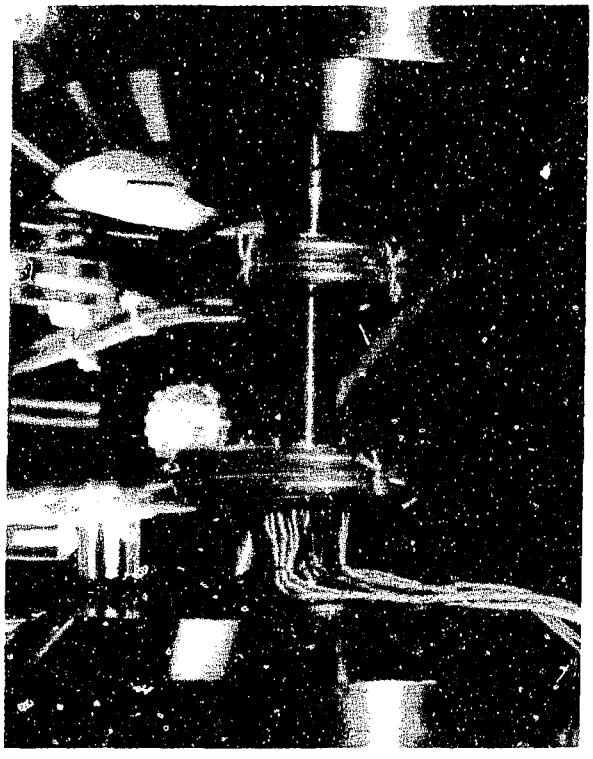

Figure 1: *View of potential drop leads and induction coil arrangement.*

To summarize, the data acquisition proceeds as follows: Mechanical data (load, strain, *etc.*) is read from the test controller and transferred to the 386 personal computer. The current is switched positive, the thermocouples are read, and following a delay, the potential drops are read. The current is switched negative and following a delay, the potential drops are reread. This cycle repeats continuously. Figure 2 (next page) shows the relationship of the test equipment and instrumentation.

During the test, the load (or torque) is plotted on an x-y flatbed plotter, and the cyclic load amplitude is checked frequently for a decrease that would warn of a crack formation. In addition, potential drop readings are displayed as they are read and a rough plot of potential drop *vs.* time is maintained by hand and checked for sudden changes. Finally, without interrupting the test, the specimen surface is visually inspected for cracks every 30 minutes using a portable 25× microscope. The test is stopped when a crack can be seen with the microscope, or with the unaided eye. However, the extensometer heat shield blocks complete visual coverage of the specimen surface. In all tests to date, the crack had grown very long before it could be seen. After the test has completed, the specimen is removed from the testing machine, and the crack length, depth and location are measured.

DATA ANALYSIS

The potential drop data consist of positive and negative values. By taking the difference between them, we compensate for changes in thermocouple emf's occurring in the potential drop leads. Also, a temperature correction is applied to compensate for specimen electrical resistivity changes due to temperature variation.

The voltage oscillates within a 150μV band (refer to subplot 1 of Figure 3). The periodic nature of the signal lends itself to standard signal processing methods [2]. First, we interpolate the data with respect to time using the low pass filter of Oetken [3], as shown in subplot 2 of Figure 3. Since we have sampled the signal at .25 Hz, which is well above the Nyquist frequency, the interpolation is accurate, and free of aliasing.

The signal oscillates within a 150μV range due to the cyclic specimen length change: In a cyclic test with a nonzero axial strain amplitude, the potential drop oscillates in phase with strain as a consequence of the standard resistance relation, $R = \rho l / A$, where l is the gauge length. The voltage oscillation dominates the signal, and makes the entire Fourier analysis possible, but is unrelated to crack size measurement, and must be accounted for. If a crack is present,

the maximum potential drop occurs at maximum crack extension; therefore we identify withing the interpolated data, the maximum per-cycle potential drop. Four such maxima are shown in subplot 3 of Figure 3. The maximum per-cycle potential drop for an entire test is shown in subplot 4 of the same figure.

The per-cycle potential drop maxima are then interpolated with respect to time using a piecewise cubic smoothing spline [4]. For a given voltmeter channel, the ratio of potential drop, $\Phi(t)$ to the starting value, $\Phi(0)$, is given by $\phi = \Phi(t)/\Phi(0)$, and is shown plotted in subplot 1 of Figure 4. The curves for the group of potential drop leads with the highest reading ϕ (probes 7, 8, and 9 in this case) are centered for clarity.

The ϕ values are interpolated again, this time with respect to time (t) and circumferential angular position (θ), accounting for the unequal potential drop lead spacing. The two dimensional tensor product spline of de Boor was used over a uniform output grid. The boundary conditions imposed on $\phi(\theta, t)$ are:

$$\phi(0, t) = \phi(2\pi, t),$$

$$\phi(\theta, 0) = \frac{d\phi}{dt}(\theta, 0) = 0.$$

Initially, the potential drops measured on all channels remain nearly level, or rise together. The rate of increase rises gradually, but uniformly.

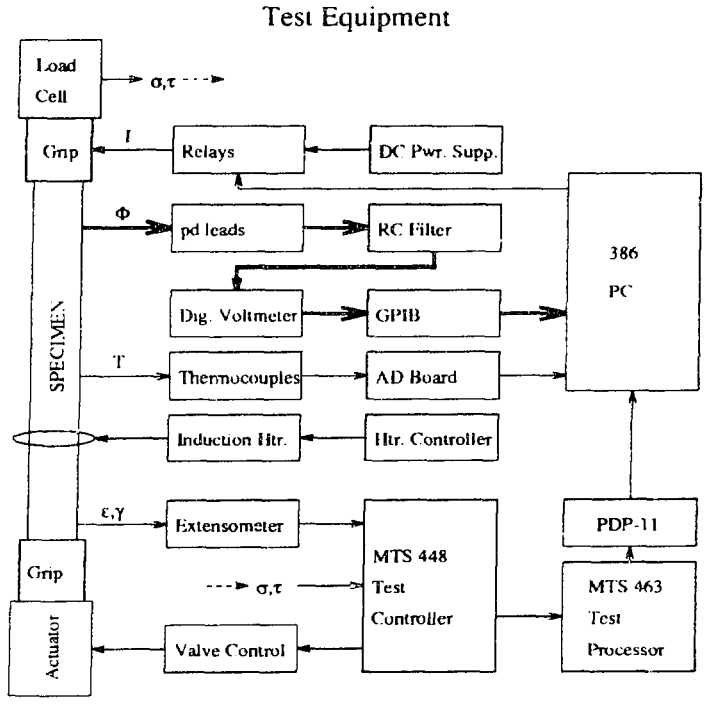

Figure 2: *Block diagram of test equipment.*

The uniform rise in potential drop may be due to the increased electrical resistance resulting from progressive surface oxidation at high temperature. Other factors, including the dislocation density increase from hardening, the formation of many uniformly distributed small cracks, or other unknown chemical and physical changes also result in a uniform potential drop rise. Eventually, a crack grows large enough to be detected and the potential drop for the probe pair closest to the crack begins to rise faster than the others. However, the crack affects the potential drop far away, too, and all potential drop readings increase faster as a result (refer to subplot 1 of Figure 4).

Clearly, we need a way to separate the local rise in ϕ due to crack growth from the general rise in ϕ which is affected by many factors in unknown proportion. Therefore, we subtract the lowest ϕ from all the others. We define the incremental normalized potential drop at time t as, $\phi_{inc}(\theta, t) = \phi(\theta, t) - \min(\phi(\theta, t))$. A crack is "detectable" when a localized rise in ϕ_{inc} is noticeable. As the crack grows, the ϕ_{inc} curve around the crack broadens and grows higher (refer to subplot 2 of Figure 4). The highest curve is centered for clarity. The y axis is arbitrarily chosen to originate from the highest curve.

We note that for the longest test (refer to Figure 5) the time required to perform the Fourier interpolation was 7:49 (wall clock, in mm:ss) on a Sun Sparc 10 model 30 with fifty users logged in at the time. An IBM Powerstation 320H performs the calculations in about the same time. The smoothing spline required 3:11 and the tensor spline interpolation required 0:07. The raw data consisted of a 15607 × 37 double precision array requiring 4.6 MB (megabytes) of memory. The largest array used was for the interpolated voltages, and required 11.2 MB of memory. The total memory requirement for the process was 41.9 MB.

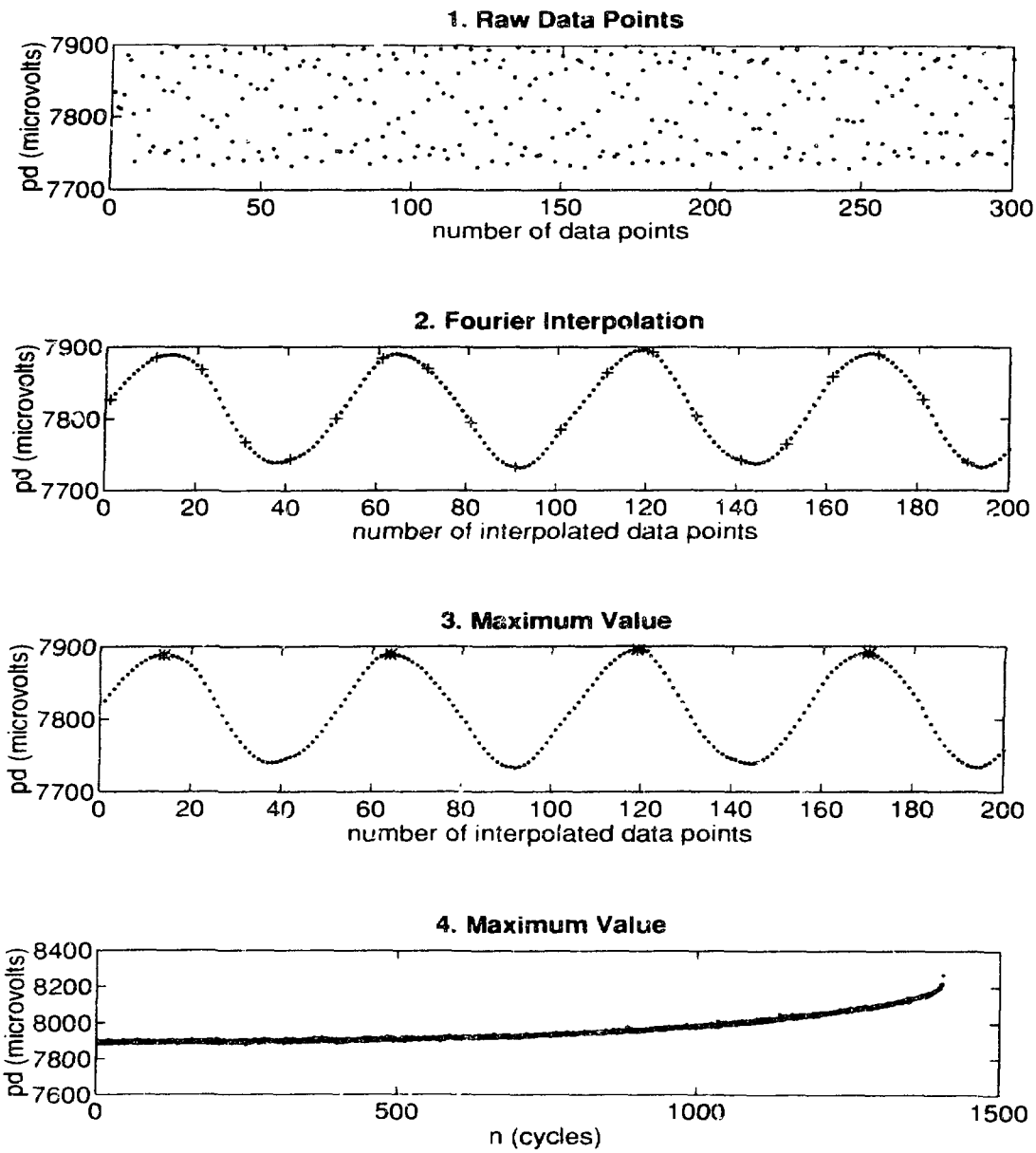

Figure 3: *Fourier analysis.* The procedure for performing the Fourier interpolation on one of nine potential drop (pd) channels is illustrated in this figure, for test c9. **1.** 300 raw data points (approximately 58 fatigue cycles) are shown. Note the false wave pattern. There appear to be five overlapping waves shown. This an artifact of the data collection method. **2.** Only 20 raw data points (+) are shown. The 10:1 Fourier interpolation is plotted with dots. **3.** The per-cycle maxima (*) of the Fourier interpolation is plotted. **4.** Subplot 3 showed only four potential drop maxima. Subplot 4 shows an entire test (N_f = 1464).

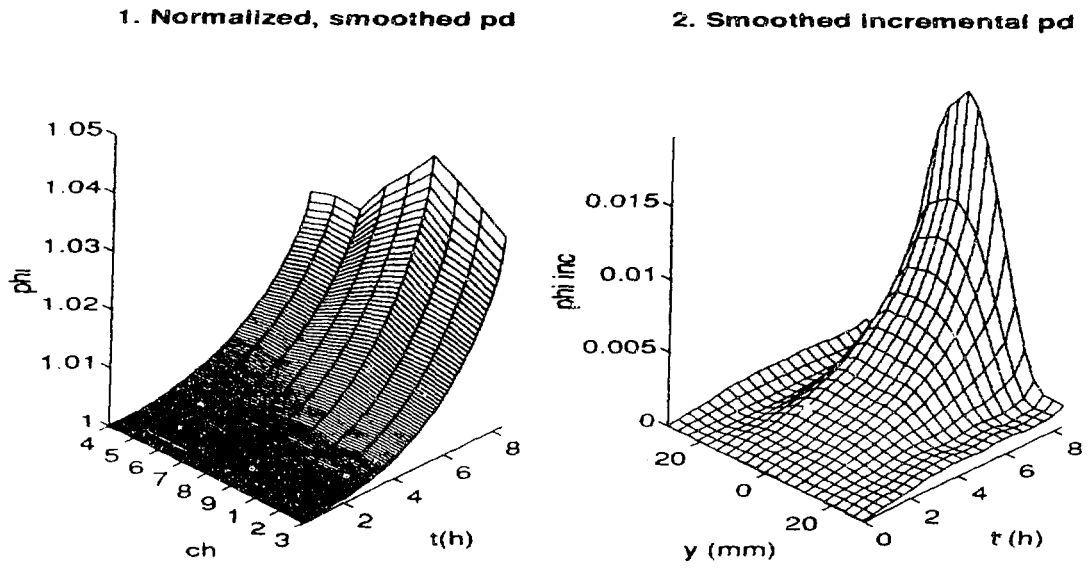

Figure 4: *Cubic spline interpolation procedure.* **1.** The pd maxima shown in subplot 4 of Figure 3 are smoothed, normalized, and interpolated at 101 time points, and plotted for all nine voltmeter channels (ch). **2.** The mesh points in subplot 1 are interpolated over a uniform mesh in two dimensions, time (t) and position (y). y is measured horizontally from the highest curve. The lowest ϕ per time step was subtracted to obtain ϕ_{inc}.

TEST RESULTS

A total of six experiments were performed and are summarized in Figure 5. Tests c6 and c7 were axial fatigue tests ($\gamma_{xy} = 0$). The follow-on tests were proportional loading tests. In tests c8 and c9 the axial and shear strain amplitudes were both .0043 and in tests d0 and d1, the axial strain amplitude was .0025 and the shear strain amplitude was .0075. It appears that the cycles-to-failure (N_f) increases as ϵ_a decreases, as might be expected. In all tests, ϕ initially rises uniformly for all channels, and as a result, ϕ_{inc} remains close to zero. This is shown on all subplots in Figure 5 as a "plateau" for the initial portion of the test. Eventually, a "hill" appears on the plot and grows and broadens. The increase in ϕ_{inc} corresponds to crack growth. In all cases, the location of the hill corresponds to the position of the crack.

For test c6, the data is shown truncated after 1443 cycles (8.08 h). After this time, the crack had grown very large, and the ϕ_{inc} for those times is too high to plot on the same scale as the portion of the test shown. For the same reason, the c7 test data is shown truncated after 265 cycles (2.67 h).

Test c7 was intended to check the effect of introducing a defect of known geometry part way into the test. After 176 cycles a .54 mm diameter, .65 mm deep hole was drilled. The result was a slight rise in ϕ_{inc}, which appears as a small upward step at $(y, t) = (0, .97)$ in subplot c7 of Figure 5. After $t = .97$h, a crack formed at the hole and grew until the test was stopped. This corresponds to the rise and spread of the curve after .97 h in the plot.

THEORETICAL POTENTIAL DROP NEAR THE CRACK

In this section, we compute the potential drop predicted by electrostatic theory for the measured final crack geometry. We will compare our potential drop measurements with Tada's solution to Laplace's equation for a semi-elliptical flat crack in a semi-infinite body [5] (refer to Figure 6). The potential at any point in the body is given by:

$$\Phi = zE_\infty \left\{ 1 + \frac{\lambda^2}{2E(k)} \int_{l^2}^{\infty} \frac{dl}{l\sqrt{l(l+1)(l+\lambda^2)}} \right\}, \qquad (1)$$

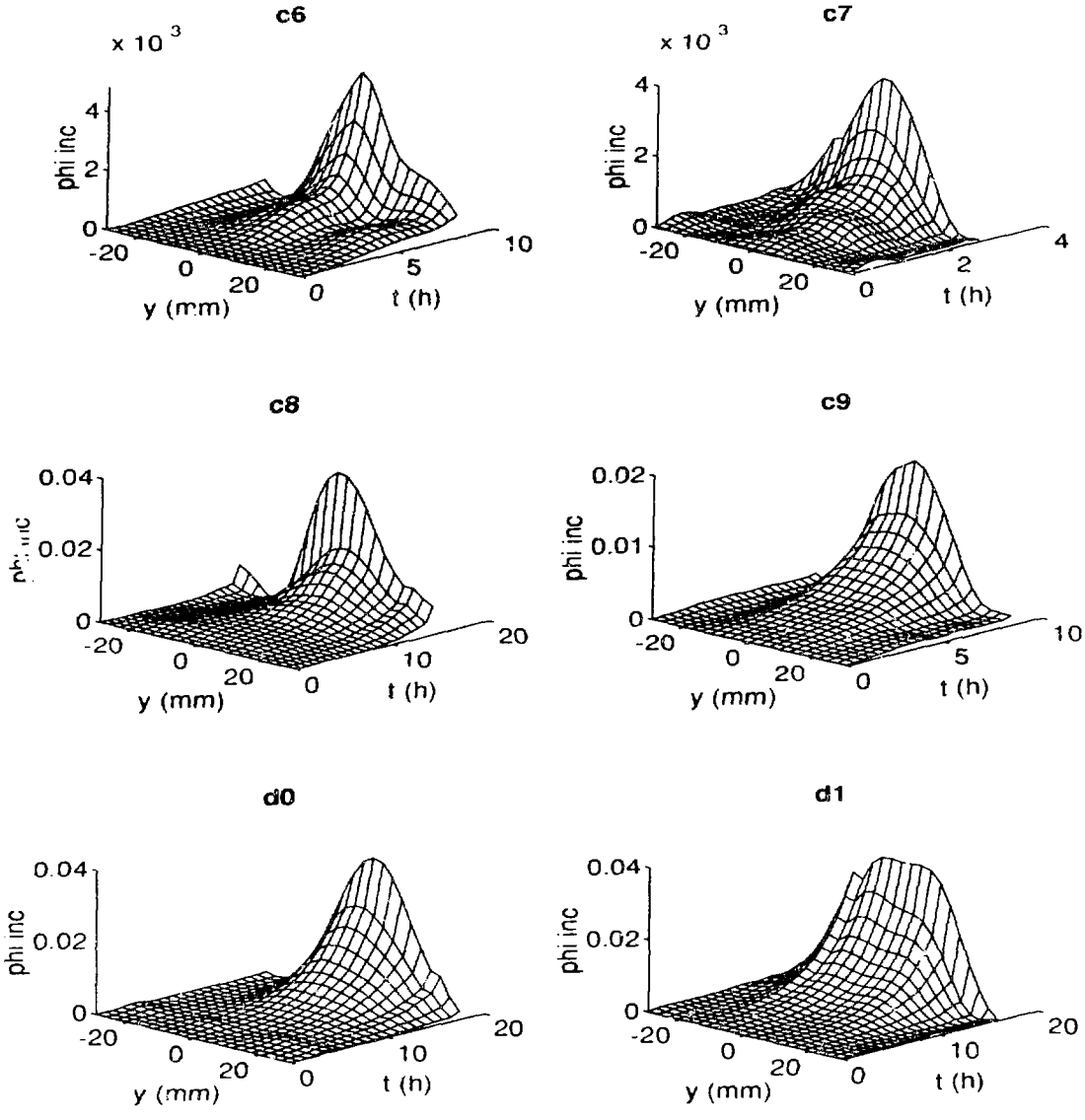

Test	ϵ_a	$\frac{1}{3}\gamma_a$	N_f	t_f (h)	$2a_f$ (mm)	ϕ_{inc}	Data file size (MB)	Number of data points
c6	.005	0	1461	8.2	37.2	4.9×10^{-3}†	1.7	7329
c7	.005	0	538	3.0	13.9	4.0×10^{-3}‡	0.7	2690
c8	.0043	0.0025	2249	13.7	19.3	3.9×10^{-2}	2.9	11640
c9	.0043	0.0025	1464	8.4	10.9	2.0×10^{-2}	1.8	7510
d0	.0025	0.0043	3021	17.5	26.1	3.9×10^{-2}	3.7	14310
d1	.0025	0.0043	2774	16.0	16.3	3.8×10^{-2}	3.4	14340

Figure 5: *Experimental results.* N_f = cycles to failure. t_f = time to failure. $2a_f$ = final crack size. ϕ_{inc} = final incremental normalized potential drop. Tests c6 and c7 were axial fatigue tests. Tests c8, c9, d0, and d1 were biaxial tests. †after 1443 cycles (8.08 h). ‡after 265 cycles (2.67 h). In test c7, a .54 mm diameter hole was drilled after 176 cycles (0.97 h) as a check on the sensitivity of the experimental technique.

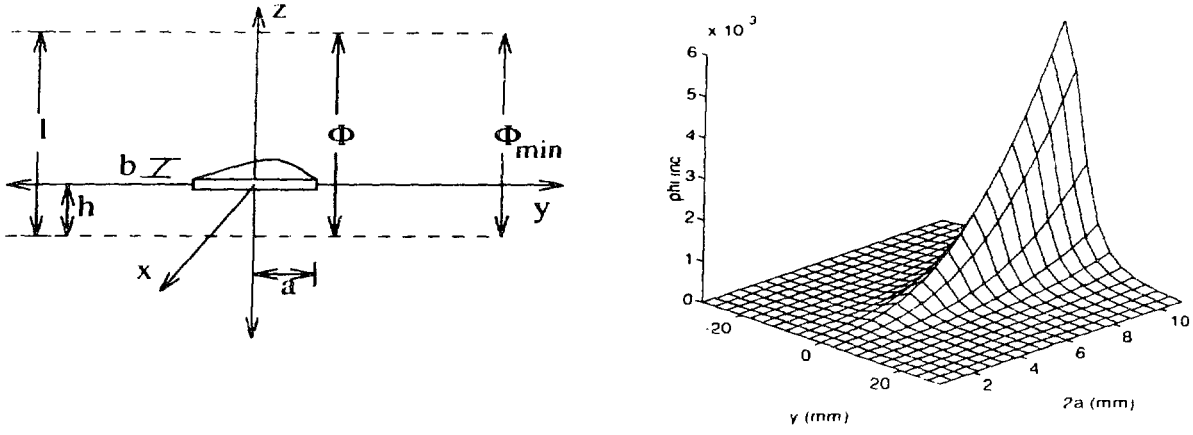

Figure 6: *Crack geometry and Tada's solution to Laplace's equation*

where E_∞ is the electric field strength at infinity, E is the complete elliptic integral of the second kind with modulus k, where $k = \sqrt{1-\lambda^2}$, λ is the crack "aspect ratio", given by $\lambda = b/a$, and D is the "effective distance" measured from the crack to the position (x, y, z), and is found by solving

$$\frac{X^2}{D^2+\lambda^2} + \frac{Y^2}{D^2+1} + \frac{Z^2}{D^2} = 1, \tag{2}$$

where $X = x/a$, $Y = y/a$, and $Z = z/a$. For surface potential measurements $x = 0$, and the solution to equation 2 is:

$$D(Y,Z) = \sqrt{\frac{Y^2+Z^2-1+\sqrt{(Y^2+Z^2-1)^2+4\cdot Z^2}}{2}}.$$

Equation 1 gives the normalized potential drop from a single voltage probe pair lead to the crack center, but a potential drop measurement is taken between *pairs* of leads. For a crack located at a distance h from the lower row of leads, the potential drop is

$$\Phi = hE_\infty \left\{1 + \frac{\lambda^2}{2E(k)} \int_{D^2_{y,h}}^{\infty} \frac{dt}{t\sqrt{t(t+1)(t+\lambda^2)}}\right\} + (l-h)E_\infty \left\{1 + \frac{\lambda^2}{2E(k)} \int_{D^2_{y,l-h}}^{\infty} \frac{dt}{t\sqrt{t(t+1)(t+\lambda^2)}}\right\}, \tag{3}$$

where $D_{y,h} = D\left(\frac{y}{a}, \frac{h}{a}\right)$ and $D_{y,l-h} = D\left(\frac{y}{a}, \frac{l-h}{a}\right)$. The observed potential drop should correspond to equation 3 only if the crack is the sole factor affecting electrical resistivity. However, it was mentioned in the Analysis section that there are many other factors that have a much greater influence on Φ than the crack does. The theoretical Φ of equation 3 includes the general rise noted on all channels, which we subtract to obtain the incremental value.

Let the minimum potential drop be Φ_{min}, calculated from equation 3 using $y = y_{max}$. In the cylindrical geometry, y_{max} is half the specimen circumference, or 14.5 mm in specimen c9, for example. If we subtract the minimum potential drop from any other potential drop, we obtain an "incremental" value. If we normalize this potential to the value that would be obtained if no crack were present, we predict:

$$\phi_{inc} = \frac{1}{l} \cdot \frac{\lambda^2}{E(k)} \left\{ h \int_{D^2_{y,h}}^{D^2_{y_{max},h}} \frac{dt}{t\sqrt{t(t+1)(t+\lambda^2)}} - (l-h) \int_{D^2_{y,l-h}}^{D^2_{y_{max},l-h}} \frac{dt}{t\sqrt{t(t+1)(t+\lambda^2)}} \right\}. \tag{4}$$

An approximate evaluation of equation 4 is plotted in Figure 6, using the measured final specimen crack geometry for test c9. In that test, a 10.9 mm crack formed 4.7 mm above the lower row of potential drop leads. The predicted ϕ for

a range of crack sizes from $2a = 0.545$ mm to the actual final value of $2a = 10.9$ mm is plotted, for a probe spacing of 25.4 mm. By the end of the test, the crack had completely breached the wall thickness (1.61 mm), so this value was used for the final semiminor axis, b, of the ellipse shown in Figure 6. A constant crack aspect ratio of $b/a = \lambda = 0.29$ was assumed for preparing the plot.

In test c9, the final experimentally determined peak value for ϕ_{nn} was 0.020 (refer to Figure 4). The peak value shown in Figure 6 is 0.006. We reconsider here the assumptions used to derive the theoretical value. A semi-infinite medium was assumed. For cracks much shorter than the specimen circumference, an infinite medium in the $\pm y$ directions is a reasonable assumption. Likewise, for cracks much shallower than the wall thickness, a semi-infinite medium in the $-x$ direction is reasonable. These assumptions would probably have been valid early in a test when the crack was small, but are poor at the end of a test because the crack is long compared to the circumference, and is completely through the wall.

CONCLUSIONS

There is qualitative agreement between the experimentally determined potential drop shown in Figure 4 and the theoretical value predicted by electrostatic theory, as shown in Figure 6. The experimentally determined ϕ_{nn} curve has the shape of a hill symmetric about the crack, and broadens and increases as the crack grows. The theoretical ϕ_{nn} has a similar shape, for crack geometry similar to the experimental one.

For the example test (c9) the final experimental ϕ_{nn} exceeds the theoretical by a factor of three because a semi-elliptical crack was assumed, but the actual final geometry was a through crack. Future work will include fitting the experimental data to other solutions to Laplace's equation, including a through crack [6]. More tests such as c7, in which a hole was drilled, will be performed. The measured potential drop will be compared to the theoretical value for the actual hole.

References

[1] W. R. Catlin, D. C. Lord, T. A. Prater, and L. F. Coffin. The reversing dc electrical potential method. In ASTM-STP877, pages 67–85, 1983.

[2] R. W. Hamming. *Digital Filters*. Prentice-Hall, Inc., Englewood Cliffs, New Jersey, 1983.

[3] G. Oetken, T. W. Parks, and H. W. Schüssler. A computer program for digital interpolator design. In *Programs for Digital Signal Processing*, chapter 8.1. IEEE Press, New York, 1979.

[4] C. de Boor. *A Practical Guide to Splines*. Springer-Verlag, New York, 1978.

[5] N. Tada. Monitoring of a surface crack in a finite body by means of electrical potential technique. *Int. J. Fract.*, 57:199–220, 1992.

[6] H. H. Johnson. Calibrating the electric potential method for studying slow crack growth. *Mater. Res. and Standards*, 5(9):442–445, 1965.